Editors' Suggestion Featured in Physics

Observation of Acoustic Skyrmions

Hao Ge,[1,*] Xiang-Yuan Xu,[2,1,*] Le Liu,[1] Rui Xu,[1] Zhi-Kang Lin,[3] Si-Yuan Yu,[1,5] Ming Bao,[2] Jian-Hua Jiang,[3,†] Ming-Hui Lu,[1,4,5,‡] and Yan-Feng Chen[1,5,§]

[1]*National Laboratory of Solid State Microstructures & Department of Materials Science and Engineering, Nanjing University, Nanjing, Jiangsu 210093, China*

[2]*Key Laboratory of Noise and Vibration Research, Institute of Acoustics, Chinese Academy of Sciences, Beijing 100190, China*

[3]*School of Physical Science and Technology, Soochow University, Suzhou 215006, China*

[4]*Jiangsu Key Laboratory of Artificial Functional Materials, Nanjing, Jiangsu 210093, China*

[5]*Collaborative Innovation Center of Advanced Microstructures, Nanjing University, Nanjing 210093, China*

(Received 12 April 2021; accepted 18 August 2021; published 29 September 2021)

Despite a long history of studies, acoustic waves are generally regarded as spinless scalar waves, until recent research revealed their rich structures. Here, we report the experimental observation of skyrmion configurations in acoustic waves. We find that surface acoustic waves trapped by a designed hexagonal acoustic metasurface give rise to skyrmion lattice patterns in the dynamic acoustic velocity fields (i.e., the oscillating acoustic air flows). Using an acoustic velocity sensing technique, we directly visualize a Néel-type skyrmion configuration of the acoustic velocity fields. We further demonstrate, respectively, the controllability and robustness of the acoustic skyrmion lattices by tuning the phase differences between the acoustic sources and by introducing local perturbations in our setup. Our study unveils a fundamental acoustic phenomenon that may enable unprecedented manipulation of acoustic waves and may inspire future technologies including advanced acoustic tweezers for the control of small particles.

DOI: 10.1103/PhysRevLett.127.144502

Introduction.—In helimagnetic materials, skyrmions emerge as stable spin textures with whirling configurations that are characterized by a real-space topological number, called the skyrmion number [1–5]. The nontrivial topology of spin textures gives rise to the stability of skyrmions. Thus, skyrmions hold promise for applications in future spintronic devices, such as data storage and logic devices, due to their extremely small size, stability, and low energy consumption in data manipulation [6–10]. Skyrmion-like vectorial textures were discovered recently in photonics [11–21] for the electric field [11,12,20] or spin [13,19] configurations of photons. Besides, skyrmion-like photonic spin textures in momentum space were also observed [18]. These discoveries unveil unconventional topological photonic modes which may be useful in robust information processing, sensing, and lasing.

The emergence of photonic skyrmions relies on the fact that photons are spin-1 particles and electromagnetic waves are vectorial [22–26]. In contrast, acoustic waves have long been regarded as spinless scalar waves that are supposed not to support skyrmion structures. Here, we demonstrate that skyrmion structures can also emerge in acoustic waves by using the velocity fields of acoustic waves. The dynamics of acoustic waves in air is described by the oscillation of the local air pressure as well as the local air flow. The latter, often denoted as the velocity fields of acoustic waves, contains key physical properties of the acoustic waves (e.g., angular momentum [27–34]), although it has been largely ignored in past studies. By exploiting the surface acoustic waves (SAWs) supported by a planner metasurface, we show that the acoustic velocity fields form a skyrmion lattice pattern that originates from the designed hexagonal symmetry of the metasurface and the evanescent nature of the SAWs. The skyrmion lattice pattern is quite stable yet can be manipulated by tuning the phase differences between the acoustic sources in our setup. We further reveal the topological robustness of the acoustic skyrmion lattice against disorders by studying the effects of local perturbations. The discovered acoustic skyrmion lattice unveils unconventional fundamental features of acoustic waves which may be useful in devices such as advanced acoustic tweezers for the manipulation of small particles.

Acoustic skyrmion number.—Skyrmions correspond to nontrivial configurations of a three-dimensional (3D) unit vector field $\vec{n}$ in a two-dimensional (2D) plane. The real-space topology is characterized by the skyrmion number S:

$$S = \frac{1}{4\pi} \iint dxdy\vec{n} \cdot (\partial_x \vec{n} \times \partial_y \vec{n}). \quad (1)$$

Nonzero skyrmion number S indicates nontrivial topology which leads to the stability of skyrmion fields.

For acoustic systems, a straightforward scheme is to utilize the velocity field, $\vec{v}$, to realize the skyrmion configurations. The velocity field stands for the oscillating velocity of the air flows, which is a key quantity in describing acoustic wave dynamics. The full wave equations for harmonic acoustic waves including the velocity field are given by

$$i\omega\rho\vec{v} = \nabla p, \quad (2)$$

$$i\omega p = \frac{1}{\rho c^2}\nabla\cdot\vec{v}, \quad (3)$$

where ω, ρ, and c are, respectively, the angular frequency of the acoustic wave, mass density, and sound velocity of the medium. The latter two can be position dependent. The above full wave equations indicate that acoustic waves are more than just spinless scalar waves. Using the velocity field $\vec{v}$, we can define the acoustic skyrmion number through Eq. (1) by setting $\vec{n} = Re(\vec{v})/|\mathrm{Re}(\vec{v})|$. The acoustic skyrmion number reflects the nontrivial warping geometry of the velocity field which may deeply affect the stability of the acoustic modes and the acoustic-matter interactions.

Realizing acoustic skyrmions through metasurfaces.—A straightforward route towards acoustic skyrmions is to utilize surface waves trapped on a 2D surface. For elastic waves in solids, Rayleigh waves trapped on 2D surfaces are a natural choice. However, for acoustic waves in air or fluids, a rigid and smooth surface cannot support 2D surface waves due to the longitudinal nature of acoustic waves. Here, we exploit an acoustic metasurface with periodically perforated holes to support the desired 2D surface waves. This type of surface waves is referred to as spoof surface acoustic waves (SSAWs), which originate from the couplings between the acoustic waves trapped by the subwavelength holes [35–41]. SSAWs are trapped by the metasurface and decay exponentially into the air region above the metasurface.

Analytically, dropping the time-dependence factor, the pressure field of a SSAW mode can be described as follows, $p = p_0 e^{i(k_x x + k_y y) - \tau z}$, if we consider only the acoustic wave function in the air region (i.e., $z > 0$) which is relevant to our experimental measurements. Here, p_0 is the wave amplitude and $(k_x, k_y) = \vec{k}_\parallel$ is the in-plane wave vector, while $1/\tau$ gives the decay constant along the z direction. The dispersion relation for the SSAWs is $k_\parallel^2 - \tau^2 = (\omega/c_0)^2$, where $k_\parallel = |\vec{k}_\parallel|$ and $c_0 = 343$ m/s is the sound velocity in air at ambient condition. From Eq. (2), one obtains that $\vec{v} = (p_0/\rho_0\omega)(k_x, k_y, i\tau)e^{i(k_x x + k_y y) - \tau z}$, where ρ_0 is the mass density of air at room temperature. The $(\pi/2)$ phase difference between the in-plane components and the z component of the acoustic velocity $\vec{v}$ indicates the possibility of creating spiral velocity fields.

To realize the acoustic skyrmions, as depicted in Fig. 1(a), we design a metasurface with hexagonal symmetry and use a setup with six pairs of speakers to excite three pairs of counterpropagating SSAWs, which form three standing waves along the $\theta = 0°$, 120°, and 240° directions. The structure of the metasurface is shown in Fig. 1(b). Each unit cell has a hole at the center with a

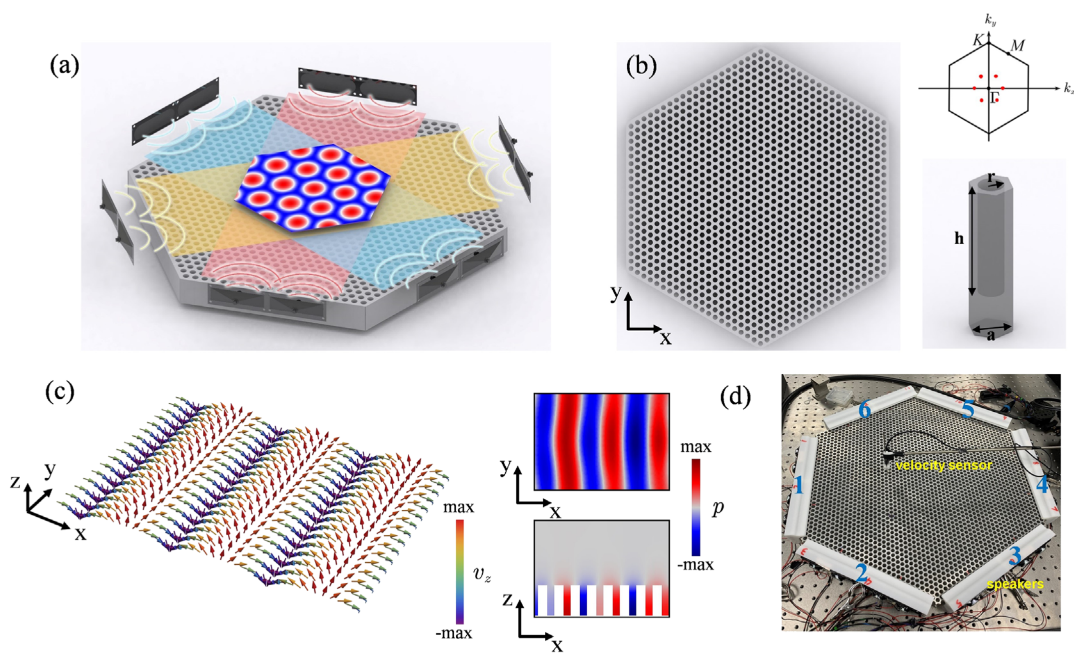

FIG. 1. Formation of acoustic skyrmions. (a) An acoustic metasurface with periodically perforated holes is utilized to support spoof surface acoustic waves (SSAWs). The interference of SSAWs excited by six pairs of speakers leads to the acoustic skyrmion lattice. (b) Structure of the acoustic metasurface. Left: top-down view. Right: the unit-cell structure of the acoustic metasurface. (c) Left: The distribution of the acoustic velocity vectors of the propagating SSAWs. Right: The distribution of the acoustic pressure field in the x-y plane (top) and the x-z plane (down). In the latter, the white region depicts the solid region of the acoustic metasurface. (d) The experimental setup where six pairs of speakers are utilized to excite the acoustic skyrmion lattice.

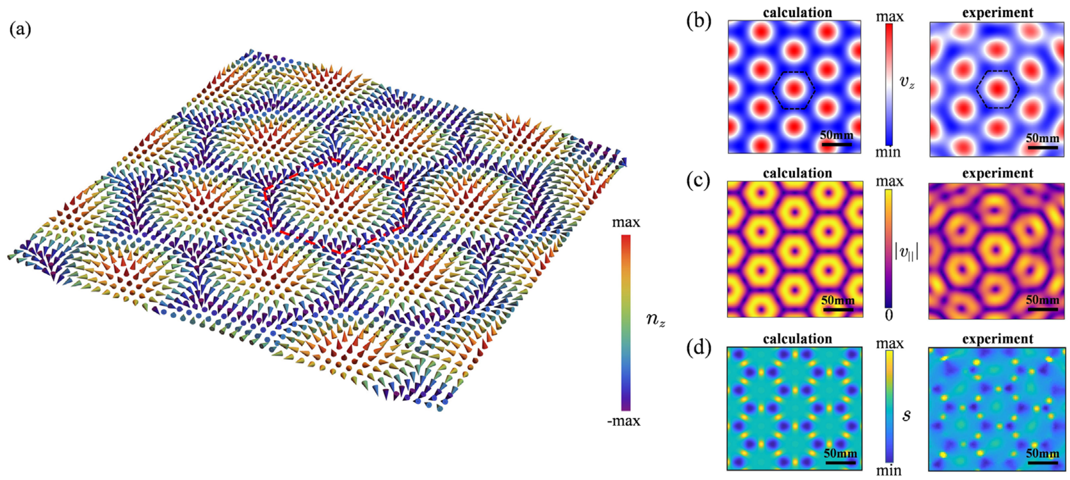

FIG. 2. Experimental observation of acoustic skyrmions. (a) Experimentally measured acoustic velocity field that exhibits features of a Néel-type skyrmion lattice pattern. Arrows indicate the normalized velocity field $\vec{n} = Re(\vec{v})/|Re(\vec{v})|$. (b) Distributions of the out-of-plane velocity field v_z from both calculation and experiments. (c) Distributions of the amplitude of the in-plane velocity field $|v_{\parallel}| = \sqrt{v_x^2 + v_y^2}$ from both calculation and experiments. (d) The skyrmion number density profile $s = \vec{n} \cdot (\partial_x \vec{n} \times \partial_y \vec{n})$ obtained from the experiments (right) together with the skyrmion number density profile obtained from the theoretical calculations (left).

radius $r = 3.3$ mm and a height $h = 30$ mm where the lattice constant is $a = 10$ mm. The velocity and pressure fields for a SSAW with $\vec{k}_{\parallel} = (0.37, 0)(\pi/a)$ are shown in Fig. 1(c), which indicate wave propagation along the x direction with spiral acoustic velocity fields and wave decay along the z direction.

Taking into account of the superposition of the three pairs of counter propagating SSAWs, the acoustic velocity fields form a skyrmion lattice pattern, which is described by the following equation,

$$\vec{v} = \frac{2p_0}{\rho_0 \omega} \sum_n (k_{n,x} \sin \vec{k}_n \cdot \vec{r}, k_{n,y} \sin \vec{k}_n \cdot \vec{r}, \tau \cos \vec{k}_n \cdot \vec{r}) e^{-\tau z}, \tag{4}$$

where $\vec{k}_n = k_{\parallel}[\cos(2n\pi/3), \sin(2n\pi/3)]$ for $n = 0, 1, 2$ and $\vec{r} = (x, y)$. The six wave vectors of the SSAWs, $\pm\vec{k}_n$, are shown as the red dots in the Brillouin zone of the metasurface in the inset of Fig. 1(b). Such a nontrivial velocity field distribution can be probed by an acoustic velocity sensor scanning on top of the metasurface in our setup [see Fig. 1(d)] (see Supplemental Material [42] for the details of the acoustic velocity sensor). In our experiments, the three pairs of counterpropagating SSAWs are excited by six pairs of speakers at the frequency of 2.37 kHz [see Figs. 1(a) and 1(d)].

Detecting acoustic skyrmions.—The skyrmion pattern of the normalized acoustic velocity field, $\vec{n} = \mathrm{Re}(\vec{v})/|\mathrm{Re}(\vec{v})|$, is shown in Fig. 2(a). Here, the skyrmion pattern defines an emergent hexagonal lattice (termed as the skyrmion lattice) with a lattice constant a_{skm} which is related to the wavelength of the SSAWs, i.e., $a_{skm} = (2/\sqrt{3}) \cdot \lambda_{SSAW} = (4\pi/\sqrt{3}k_{\parallel})$. The unit cell of the emergent skyrmion lattice is depicted by the dashed hexagons in Figs. 2(a) and 2(b) where the out-of-plane acoustic velocity v_z reaches its maximum value at the center of each skyrmion unit cell. Within such a unit cell, the skyrmion number of the velocity field is $S = 1$. We remark that, although the velocity field oscillates as a function of time, its amplitude and phase can be well captured by using a data acquisition module in our experiments. The 3D velocity field on the 2D metasurface is measured by an acoustic velocity sensor mounted on a moving stage (with steps of 2.5 mm in both the x and y directions). We use the velocity sensor to detect the amplitude and the phase of the x, y, and z components of the velocity field separately, and then use these data to construct the distribution of the acoustic velocity vector (see details in the Supplemental Material [42]).

The measured distribution of the normalized acoustic velocity field, $\vec{n}$, in Fig. 2(a) indicates a clear feature of a Néel type skyrmion. Although the excited acoustic waves are not perfect plane waves and they suffer acoustic attenuations due to the intrinsic thermoacoustic damping, remarkably, the experimental results clearly demonstrate the formation of an acoustic skyrmion lattice. The calculated and measured distributions of the out-of-plane and in-plane acoustic velocity components, v_z and $|v_{\parallel}| = \sqrt{v_x^2 + v_y^2}$, are shown in Figs. 2(b) and 2(c), respectively. For these two components, the measured distributions of the acoustic velocity agree fairly well with the calculated distributions, confirming the emergence of the skyrmion lattice pattern. In Fig. 2(d), we present the skyrmion number density profile $s = \vec{n} \cdot (\partial_x \vec{n} \times \partial_y \vec{n})$ extracted from the experimental data together with the skyrmion number density profile obtained from the theoretical calculations. These two profiles agree with each other as well. The skyrmion number S is the integral of the skyrmion number density over a unit cell of the emergent skyrmion lattice. The experimentally extracted average skyrmion number of the seven unit cells in the central region of the system is $S = 0.956$, which is fairly close to the theoretical value of $S = 1$.

Manipulation of acoustic skyrmion lattices.—We now demonstrate how to manipulate the acoustic skyrmion lattice by controlling the phases of the six pairs of speakers. The acoustic skyrmion lattice is formed by the interference of the SSAWs excited by the speakers and can thus be manipulated by the phases of the six pairs of speakers, which are denoted here as ϕ_m with $m = 1, \ldots, 6$. The six pairs of speakers are numerated according to Figs. 1(d) and 3(a). We investigate two prototype configurations, I and II. In configuration I, the phases of the six pairs of speakers are set as the same, i.e., $\phi_m = 0$ for $m = 1, \ldots, 6$. For this case, the measured lattice pattern of the out-of-plane acoustic velocity v_z is given in Fig. 3(a). In configuration II, we set the phases as $\phi_1 = -\phi_4 = \pi$, $\phi_2 = \phi_6 = (\pi/2)$, $\phi_3 = \phi_5 = -(\pi/2)$. For this case, the measured lattice pattern of the out-of-plane acoustic velocity v_z is given in Fig. 3(b), which shows that the skyrmion lattice moves along the (white) horizontal arrow by a distance of $\frac{1}{2}\lambda_{SSAW}$. The shift of the skyrmion lattice can also be observed by measuring the in-plane velocity amplitude, as shown in Figs. 2(c) and 2(d). Tuning the phases of the six pairs of speakers will not distort the skyrmion lattice but only shifting the skyrmion lattice pattern if the phases satisfy certain relations (see details in Supplemental Material [42]). The distance and the direction of the pattern shifting is determined by the phases ϕ_m with $m = 1, \ldots, 6$. Therefore, these phases behave as the emergent degrees of freedom for the skyrmion lattices. Besides, the shape of acoustic skyrmions can also be tailored by tuning the amplitude of the incident acoustic waves [21]. For instance, increasing the amplitude of the standing wave in one direction leads to the deformation of the acoustic skyrmion lattice (see details in Supplemental Material [42]).

Robustness of acoustic skyrmion lattices.—The nontrivial real-space topology of the acoustic skyrmion lattice gives rise to the robustness of the acoustic velocity textures. As shown in Fig. 4(a), we intentionally introduce defects on the acoustic metasurface by using eight screws to block the air holes near the center of the sample. These defects lead to the scattering of the SSAWs and thus distort the skyrmion lattice pattern of the acoustic velocity field. However, experimental results shown in Fig. 4(b) indicate that the skyrmion lattice pattern is negligibly affected by the defects. Careful examination of the out-of-plane and in-plane acoustic velocity fields in Figs. 4(c) and 4(d) indicates that the acoustic velocity field patterns are only slightly modified near the defects. With such strong defect

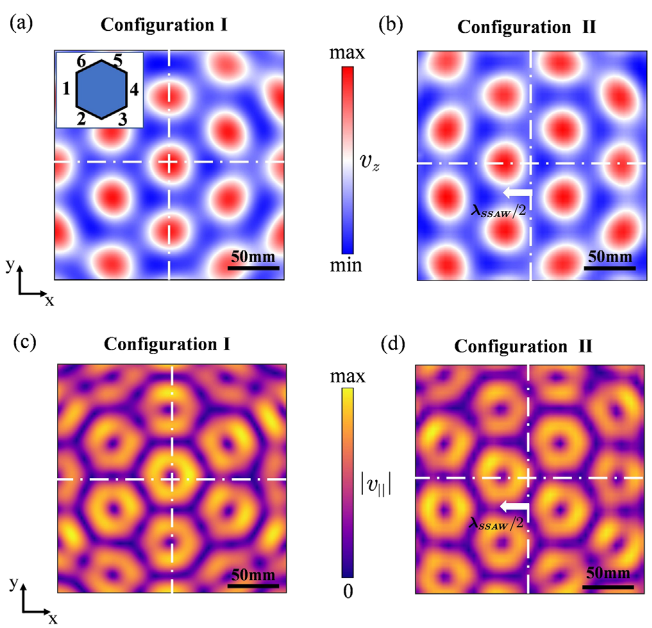

FIG. 3. Manipulation of acoustic skyrmion lattices by tuning the phases of the SSAWs excited by the six pairs of speakers at the boundaries [marked by 1–6 in the inset of (a)]. Two cases, denoted as configuration I and II (see details in the main text), are measured. (a) and (b), the out-of-plane velocity fields v_z for the configuration I and II, respectively. (c) and (d), the in-plane velocity fields $|v_{\parallel}|$ for the configuration I and II, respectively.

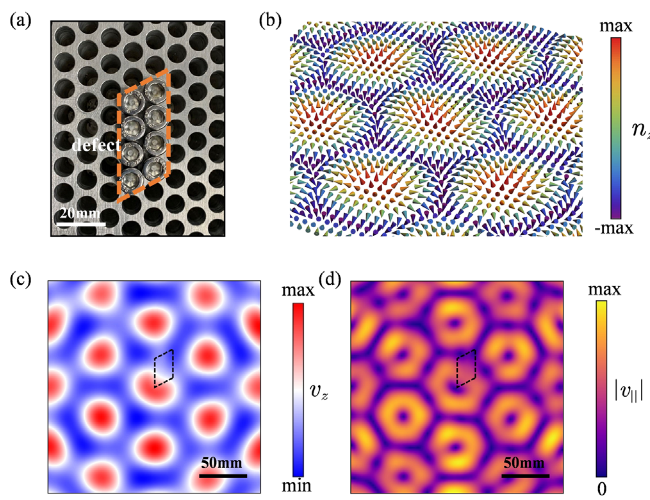

FIG. 4. Robustness of the acoustic skyrmion lattice. (a) A defect made of eight screws blocking the air holes is placed on the metasurface sample, which causes scattering of the acoustic waves and distort the acoustic fields. (b) Experimentally measured acoustic velocity field for the sample with the defect. The acoustic skyrmion lattice is negligibly affected. Arrows indicate the normalized velocity field $\vec{n} = Re(\vec{v})/|Re(\vec{v})|$. (c) and (d) The measured out-of-plane and in-plane velocity field distributions, showing slight deformations near the defect (the dashed parallelogram).

effect, the experimentally extracted average skyrmion number of the seven skyrmion unit-cells in the central region of the system is $S = 0.963$, which has very little change compared with the original value $S = 0.956$ for the system without the defect. These experimental results confirm that the acoustic skyrmions are robust against the defects.

Conclusion and outlook.—In conclusion, by designing an acoustic metasurface with hexagonal symmetry, we successfully create a skyrmion lattice of the acoustic velocity fields which can be manipulated by the amplitudes and phases of the three standing waves excited by six pairs of speakers. The acoustic skyrmion lattice is shown to be robust against defects and disorders. This work highlights the commonly ignored vectorial properties of acoustic waves which will thus deepen the understanding of acoustic waves and inspire future studies on more real-space topological structures in acoustic waves, such as Bloch-type skyrmions, anti-skyrmions, and merons [18,43–45]. The stability and tunability of the acoustic skyrmion lattice make it promising in near-field acoustic applications based on metasurfaces, such as manipulation of small particles [30]. The acoustic skyrmions can also be applied in high-frequency surface acoustic wave tweezers based on piezoelectric substrates, which are capable of performing dynamic manipulation of micro-objects [46,47].

The work is jointly supported by the National Key R&D Program of China (Grants No. 2017YFA0303702, No. 2017YFA0305100, and No. 2018YFA0306200), the National Natural Science Foundation of China (Grants No. 11804149, No. 11625418, No. 11890702, No. 51721001, and No. 12074281). We also acknowledge the support of the Natural Science Foundation of Jiangsu Province, Jiangsu specially appointed professor funding, and the support from the Priority Academic Program Development of Jiangsu Higher Education (PAPD).

*These authors contributed equally to this work.
†Corresponding author.
joejhjiang@hotmail.com
‡Corresponding author.
luminghui@nju.edu.cn
§Corresponding author.
yfchen@nju.edu.cn

[1] T. H. R. Skyrme, Nucl. Phys. **31**, 556 (1962).
[2] U. K. Rößler, A. N. Bogdanov, and C. Pfleiderer, Nature (London) **442**, 797 (2006).
[3] S. Mühlbauer, B. Binz, F. Jonietz, C. Pfleiderer, A. Rosch, A. Neubauer, R. Georgii, and P. Böni, Science **323**, 915 (2009).
[4] X. Z. Yu, Y. Onose, N. Kanazawa, J. H. Park, J. H. Han, Y. Matsui, N. Nagaosa, and Y. Tokura, Nature (London) **465**, 901 (2010).
[5] S. Heinze, K. von Bergmann, M. Menzel, J. Brede, A. Kubetzka, R. Wiesendanger, G. Bihlmayer, and S. Blügel, Nat. Phys. **7**, 713 (2011).
[6] J. Sampaio, V. Cros, S. Rohart, A. Thiaville, and A. Fert, Nat. Nanotechnol. **8**, 839 (2013).
[7] A. Fert, V. Cros, and J. Sampaio, Nat. Nanotechnol. **8**, 152 (2013).
[8] N. Nagaosa and Y. Tokura, Nat. Nanotechnol. **8**, 899 (2013).
[9] N. Romming, C. Hanneken, M. Menzel, J. E. Bickel, B. Wolter, K. von Bergmann, A. Kubetzka, and R. Wiesendanger, Science **341**, 636 (2013).
[10] A. Fert, N. Reyren, and V. Cros, Nat. Rev. Mater. **2**, 17031 (2017).
[11] S. Tsesses, E. Ostrovsky, K. Cohen, B. Gjonaj, N. H. Lindner, and G. Bartal, Science **361**, 993 (2018).
[12] S. Tsesses, K. Cohen, E. Ostrovsky, B. Gjonaj, and G. Bartal, Nano Lett. **19**, 4010 (2019).
[13] L. Du, A. Yang, A. V. Zayats, and X. Yuan, Nat. Phys. **15**, 650 (2019).
[14] K. Wang, X. Qiu, L. Xiao, X. Zhan, Z. Bian, B. C. Sanders, W. Yi, and P. Xue, Nat. Commun. **10**, 2293 (2019).
[15] T. Van Mechelen and Z. Jacob, Opt. Mater. Express **9**, 95 (2019).
[16] Y. Dai, Z. Zhou, A. Ghosh, K. Kapoor, M. Dąbrowski, A. Kubo, C.-B. Huang, and H. Petek, arXiv:1912.03826.
[17] Q. Zhang, Z. Liu, F. Qin, S. J. Zeng, D. Zhang, Z. Gu, X. Liu, and J. J. Xiao, Opt. Express **27**, 7009 (2019).
[18] C. Guo, M. Xiao, Y. Guo, L. Yuan, and S. Fan, Phys. Rev. Lett. **124**, 106103 (2020).
[19] P. Shi, L. Du, and X. Yuan, Nanophotonics **9**, 4619 (2020).
[20] T. J. Davis, D. Janoschka, P. Dreher, B. Frank, F. J. Meyer Zu Heringdorf, and H. Giessen, Science **368**, eaba6415 (2020).
[21] C. Bai, J. Chen, Y. Zhang, D. Zhang, and Q. Zhan, Opt. Express **28**, 10320 (2020).
[22] A. Aiello, P. Banzer, M. Neugebauer, and G. Leuchs, Nat. Photonics **9**, 789 (2015).
[23] K. Y. Bliokh and F. Nori, Phys. Rep. **592**, 1 (2015).
[24] K. Y. Bliokh, F. J. Rodríguez-Fortuño, F. Nori, and A. V. Zayats, Nat. Photonics **9**, 796 (2015).
[25] K. Y. Bliokh, D. Smirnova, and F. Nori, Science **348**, 1448 (2015).
[26] L. Peng, L. Duan, K. Wang, F. Gao, L. Zhang, G. Wang, Y. Yang, H. Chen, and S. Zhang, Nat. Photonics **13**, 878 (2019).
[27] C. Shi, R. Zhao, Y. Long, S. Yang, Y. Wang, H. Chen, J. Ren, and X. Zhang, Natl. Sci. Rev. **6**, 707 (2019).
[28] K. Y. Bliokh and F. Nori, Phys. Rev. B **99**, 174310 (2019).
[29] K. Y. Bliokh and F. Nori, Phys. Rev. B **99**, 020301(R) (2019).
[30] I. D. Toftul, K. Y. Bliokh, M. I. Petrov, and F. Nori, Phys. Rev. Lett. **123**, 183901 (2019).
[31] Y. Long, H. Ge, D. Zhang, X. Xu, J. Ren, M.-H. Lu, M. Bao, H. Chen, and Y.-F. Chen, Natl. Sci. Rev. **7**, 1024 (2020).

[32] Y. Long, D. Zhang, C. Yang, J. Ge, H. Chen, and J. Ren, Nat. Commun. **11**, 4716 (2020).

[33] L. Burns, K. Y. Bliokh, F. Nori, and J. Dressel, New J. Phys. **22**, 053050 (2020).

[34] J. H. Lopes, E. B. Lima, J. P. Leao-Neto, and G. T. Silva, Phys. Rev. E **101**, 043102 (2020).

[35] J. Christensen, A. I. Fernandez-Dominguez, F. de Leon-Perez, L. Martin-Moreno, and F. J. Garcia-Vidal, Nat. Phys. **3**, 851 (2007).

[36] Y. Zhou, M.-H. Lu, L. Feng, X. Ni, Y.-F. Chen, Y.-Y. Zhu, S.-N. Zhu, and N.-B. Ming, Phys. Rev. Lett. **104**, 164301 (2010).

[37] J. Zhu, J. Christensen, J. Jung, L. Martin-Moreno, X. Yin, L. Fok, X. Zhang, and F. J. Garcia-Vidal, Nat. Phys. **7**, 52 (2011).

[38] D. Torrent and J. Sanchez-Dehesa, Phys. Rev. Lett. **108**, 174301 (2012).

[39] H. Jia, M. Lu, Q. Wang, M. Bao, and X. Li, Appl. Phys. Lett. **103**, 103505 (2013).

[40] L. Schwan, A. Geslain, V. Romero-García, and J.-P. Groby, Appl. Phys. Lett. **110**, 051902 (2017).

[41] T. Liu, F. Chen, S. Liang, H. Gao, and J. Zhu, Phys. Rev. Applied **11**, 034061 (2019).

[42] See Supplemental Material at http://link.aps.org/supplemental/10.1103/PhysRevLett.127.144502 for discussions about the acoustic particle velocity sensing technique, manipulation of skyrmion lattice, skyrmion number in each unit-cell, introducing larger perturbations, and the skyrmion number density distribution for different transverse wave vectors.

[43] X. Z. Yu, W. Koshibae, Y. Tokunaga, K. Shibata, Y. Taguchi, N. Nagaosa, and Y. Tokura, Nature (London) **564**, 95 (2018).

[44] A. K. Nayak, V. Kumar, T. Ma, P. Werner, E. Pippel, R. Sahoo, F. Damay, U. K. Rößler, C. Felser, and S. S. P. Parkin, Nature (London) **548**, 561 (2017).

[45] Q. Zhang, Z. Xie, L. Du, P. Shi, and X. Yuan, Phys. Rev. Research **3**, 023109 (2021).

[46] Z. Tian *et al.*, Sci. Adv. **5**, eaau6062 (2019).

[47] P. Zhang, H. Bachman, A. Ozcelik, and T. J. Huang, Annu. Rev. Anal. Chem. **13**, 17 (2020).